RESEARCH ARTICLE

WILEY

Self-sealing thermoplastic fluoroelastomer enables rapid fabrication of modular microreactors

Alexander H. McMillan[1,2] | **Juan Mora-Macías**[3] | **Joan Teyssandier**[4] |
Raymond Thür[2] | **Emmanuel Roy**[5] | **Ignacio Ochoa**[6] | **Steven De Feyter**[4] |
Ivo F. J. Vankelecom[2] | **Maarten B. J. Roeffaers**[2] | **Sasha Cai Lesher-Pérez**[1]

[1] Elvesys Microfluidics Innovation Center, Paris, France

[2] Department of Microbial and Molecular Systems, Centre for Membrane Separations, Adsorption, Catalysis and Spectroscopy for Sustainable Solutions (cMACS), KU Leuven, Leuven, Belgium

[3] Department of Mining, Mechanical, Energy and Construction Engineering, University of Huelva, Huelva, Spain

[4] Division of Molecular Imaging and Photonics, Department of Chemistry, KU Leuven, Leuven, Belgium

[5] Eden Tech SAS, Paris, France

[6] Tissue Microenvironment Lab (TME), Aragón Institute of Engineering Research (I3A, Institute for Health Research Aragon (IIS Aragón, Biomedical Research Networking Center in Bioengineering Biomaterials and Nanomedicine (CIBER-BBN), University of Zaragoza, Zaragoza, Spain

Correspondence
Sasha Cai Lesher-Pérez, Elvesys Microfluidics Innovation Center, 75011 Paris, France.
Email: sashacai.lesherperez@gmail.com

Funding information
H2020 Marie Skłodowska-Curie Actions, Grant/Award Numbers: 722591, 753743; Horizon 2020 Framework Programme, Grant/Award Number: 829010

Abstract

A novel fluorinated soft thermoplastic elastomer (sTPE) for microfluidics is presented. It allows the rapid fabrication of microfluidic devices through a 30-second hot embossing cycle at 220°C followed by self-sealing through simple conformal contact at room temperature, or with baking. The material shows high chemical resistance, particularly in comparison to polydimethylsiloxane (PDMS), to many common organic solvents and can be rapidly micropatterned with high fidelity using a variety of microfluidic master molds thanks to its low mechanical stiffness. Self-sealing of the material is reversible and withstands pressures of up to 2.8 bar with room temperature sealing and four bar with baking at 185°C for 2 hours. The elastomeric, transparent sTPE exhibits material characteristics that make it suited for use as a microreactor, such as low absorption, surface roughness and oxygen permeability, while also allowing a facile and scalable fabrication process. Modular microfluidic devices, leveraging the fast and reversible room temperature self-sealing, are demonstrated for the generation of water droplets in a toluene continuous phase using T-junctions of variable size. The sTPE offers an alternative to common microfluidic materials, overcoming some of their key drawbacks, and giving scope for low-cost and high-throughput devices for flow chemistry applications.

KEYWORDS
flow chemistry, microreactor, modular microfluidics, rapid fabrication, soft thermoplastic elastomer, solvent resistance

1 | INTRODUCTION

While the evolution of microfluidics has placed an emphasis on its use as a tool for biological research,[1] the initial emergence of microfluidic technology touted its use for chemical analysis and synthesis.[2–6] Indeed, the physical characteristics of fluids at the micro scale can provide for chemical syntheses with greater speed[7] and selectivity,[8] while also permitting safer[9] and more sustainable reactions[10,11] as compared to batch chemistry methods. The implementation of microfluidic systems in chemical synthesis never proliferated in the same fashion as in biological studies.[12] While there are numerous factors as to why, one key bottleneck has been the selection of a material with suitable properties for the demands of flow chemistry that also permits an easily adoptable method of microfluidic device fabrication.

Flow chemists using microfluidic devices have traditionally stuck to what is familiar, most often opting for glass devices, which demonstrate excellent chemical inertness, heat resistance and optical clarity. The tradeoff for glass devices is their higher material cost and more expensive and intensive fabrication methods as compared to those of polymeric materials.[13] Furthermore, glass microdevice fabrication most often entails the use of dangerous chemicals (such as hydrofluoric acid or potassium hydroxide), whereby stringent, and costly, safety measures must be put in place to ensure proper handling, disposal, and clean-up. The multi-step process of glass wet etching[14] requires sophisticated equipment and expertise, and results in a large time investment for individual devices. While alternative methods of glass micropatterning exists, such as micromachining,[15] laser-assisted material modification[16–18] and deep reactive ion etching,[19] they do not significantly improve the ease or speed of device fabrication. The accumulation of cost and fabrication time further increases with subsequent bonding of glass devices, which can be accomplished through adhesives,[20] anodic bonding,[21] high temperatures and pressures[22,23] or chemical washing.[24,25] The work-flow of glass microfluidic device processing and development can make it inaccessible to labs in lower-resource settings.

A transition to plastic devices in flow chemistry that addresses the costly and intensive fabrication of glass devices is a complicated endeavor that has not yet been fully realized. Most polymeric materials championed in microfluidics are those used in biological applications. This includes polydimethylsiloxane (PDMS), polystyrene (PS) and polycarbonate (PC), which are incompatible with many organic solvents.[26,27] Organic solvents cause these materials to swell or dissolve entirely, leading to microchannel deformation in minor cases and complete device failure in more serious cases.[26,28]

Fluoropolymers, however, offer higher chemical resistance than that of most other plastics[29,30] and have been used for microfluidic devices through 3D printing,[31] xurography,[32] hot embossing,[33,34] micromachining[35] and photocurable molding,[36] as well as in solvent resistant coatings for PDMS channels.[37,38] Despite successfully achieving solvent resistant polymeric microfluidic devices, predominantly using polytetrafluoroethylene (PTFE), none of these techniques has been widely adopted for flow chemistry applications. This is likely due to some fabrication complexities that persist in these techniques, such as limited resolution, high initial costs and low-throughput production that is not easily transferable to large-scale employment. While these techniques are variable in their strengths and drawbacks, they all share a challenge associated with bonding – a common difficulty faced when working with fluoropolymers. The most promising microfabrication methodologies rely on the addition of adhesive layers for sealing[33,39] or thermal bonding,[32,34] which introduces complications of channel collapse or deformation without careful optimization of bonding procedures.

The emergence of soft thermoplastic elastomer (sTPE) materials, such as Flexdym [40–42] and Versaflex CL30,[43] has made steps in bridging the gap between the fabrication accessibility of elastomeric materials (like PDMS) and the high-throughput production potential of thermoplastics.[44] These materials have principally been composed of styrenic co-polymers, which have favorable material properties for biological applications. Moreover they can be processed to make microfluidic devices through rapid hot embossing and facile self-sealing through conformal contact,[40] thanks in part to their soft, elastomeric properties. This self-sealing is a reversible process that avoids the additional measures for bonding that are required by other thermoplastics and that have persistently limited the more widespread adoption of thermoplastic devices.[45] These sTPEs can be inexpensively and quickly made into devices in small lab settings, but very critically possess the same scale-up potential as traditional hard plastics through techniques like injection molding and roll-to-roll hot embossing. Consequently, the same material can be implemented across manufacturing scales, in both research-scale development and industrial-scale implementation. This fabrication transferability of sTPEs sharply contrasts with hard thermoplastics, which most often require robust and expensive master molds that must handle high temperatures and pressures and withstand de-molding from rigid substrates.[46,47] The resulting cost and processing expertise becomes largely infeasible for small labs and rapid prototyping, posing a significant bottleneck in microfluidics' transition between research and industry with hard plastics. While these

existing sTPE materials have been shown to be effective for biological applications, their material composition suggests chemical resistance similar to that of polystyrene,[48] thus unsuitable for most flow chemistry applications in which organic solvents are used.

In this work, we introduce Fluoroflex (Eden Tech), a new fluoroelastic terpolymer Poly(TFE-*ter*-E-*ter* HFP) material which is melt processable, transparent and features enhanced self-sealing properties (TFE = tetrafluoroethylene, E = ethylene, HFP = hexafluoropropylene). We evaluate the sTPE's resistance to a variety of common organic solvents by swelling testing, and further characterize the material's optical, mechanical and surface properties in addition to investigating its absorption of small molecules and oxygen permeability. A microfabrication protocol was developed, allowing the rapid and facile production of microfluidic devices with a hot embossing cycle of less than 1 minute followed by self-sealing via conformal contact. Finally, a modular Fluoroflex device is used for variable size droplet generation to demonstrate the utility of its fast and reversible self-sealing, highlighting the polymer's potential as a solvent resistant material for flow chemistry microreactors with highly transferable fabrication characteristics.

2 | RESULTS AND DISCUSSION

2.1 | sTPE microfabrication

2.1.1 | Hot embossing

Raw Fluoroflex material is processed in an extruded pellet form, requiring a thermoforming procedure to achieve a functional microfluidic device. Fluoroflex exhibits a melting temperature of approximately 210°C –220°C. Attempted hot embossing at 200°C produced a crumbling effect on the polymer pellets, as opposed to pure melting behavior. 220°C was found to be the minimum temperature at which reliable hot embossing molding could be achieved. At temperatures above the polymer melt/flow temperature, the material essentially acts as a liquid, capable of filling sub-micrometric spaces (analogous to liquid PDMS prepolymer-crosslinker during soft lithography). While the lower limit of Fluoroflex channel and feature dimensions was not explicitly evaluated, the theoretical limit possible is in the sub-micrometer range.

sTPE pellets were uniformly placed between a microfluidic master mold and a smooth rigid surface (glass slide, silicon wafer or polished metal plate) opposite the mold to act as a counter-plate for hot embossing. sTPE hot embossing was performed with a manual heat press at 220°C by applying pressure for approximately 15 seconds, or until the melted polymer propagated across the desired area of hot embossing. Pressure was then released and the mold assembly was removed from the heat press and left at room temperature to cool for 1 minute before removal of the counter-plate. The sTPE sheet itself could subsequently be removed easily from the master mold. The 1-minute cooling window allows enough time for the polymer to cool below its melt/flow-temperature of ~220°C. Without this wait time, the mechanical integrity of the micropatterned polymer sheet is not maintained, whereby attempted removal of the sheet results in tearing and/or plastic deformation. The same procedure was repeated with a plain glass slide in place of the master mold in order to obtain un-patterned sTPE sheets as the complementary, bottom layer for microfluidic device sealing.

The developed hot embossing protocol was used to create micropatterned sheets of the Fluoroflex polymer within 30 seconds (Figure 1A). Half of this time, ~15 seconds, is spent to heat both the mold and counter-plate of the assembly before pressure is applied through the press. Without this step, the polymer pellets were found to produce less uniform melt distribution, sometimes resulting in air bubbles in the final micropatterned sTPE sheet. The time of the assembly under pressure could be varied depending on the desired thickness of the final sTPE sheet. Spacers could be placed between the two heated plates to control for the final hot embossed sTPE sheet thickness. A pressing time of 15 seconds was sufficient for producing sTPE sheets of between 0.5 and 1 mm thickness, whereas ~100 μm films could be fabricated by removing spacers and pressing for 30 seconds. These thin, elastomeric films could feasibly be used for the implementation of on-chip pneumatic "Quake" valves.[49] Hot embossed sTPE sheets can be stored indefinitely for subsequent manipulation or bonding, with no degradation observed throughout the duration of this work. Step-by-step images of the sTPE hot embossing process are shown in Figure S1.

In this work, two types of microfluidic master mold were used for hot embossing micropatterned sTPE: an electroformed nickel-cobalt mold and dry film photoresist-based molds. While the metallic mold is representative of a hot embossing mold for hard thermoplastics, Fluoroflex's elastomeric properties permit the use of less robust molds on glass slides or silicon wafer substrates. The dry film photoresist molds, consisting of Ordyl photoresist on glass slides, represent a fast and inexpensive means of microfluidic molding.[50] Fluoroflex's versatility in molding is consistent with that of previously reported sTPEs, and highlights the transferability of such materials; they present a PDMS-like low investment threshold for small-scale implementation, but also possess the scope for large-scale production of thermoplastics.
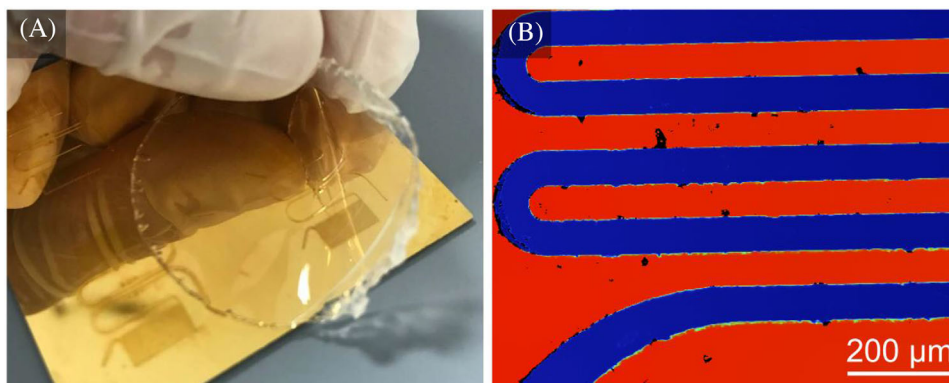
FIGURE 1 A, Removal of a sheet of Fluoroflex from a nickel-cobalt microfluidic mold after hot embossing for under 30 seconds to create micro-patterned Fluoroflex sheets, which can be subsequently assembled into microfluidic devices through self-sealing. B, Profilometer image of serpentine channels (70 μm, 1:1 aspect ratio) patterned into Fluoroflex with nickel-cobalt mold, exhibiting mold-chip fidelity of approximately 3 μm, or less than 5% difference. Dark spots between channels likely indicate the presence of dust particles on the sTPE sheet

While hot embossing equipment is not currently commonplace in microfluidics labs, the cost of hot embossing equipment is rather modest as compared to equipment in traditional microfluidic work flows (e.g., 2000–3000 EUR for the manual heat press used in this study). The hot embossing procedure is compatible with typical microfluidic master molds and, outside of a heat press, does not require further equipment beyond what exists in a standard microfluidic soft lithography work flow, namely an oven. That being said, an alternative method of Fluoroflex micropatterning could be envisioned by adding weight atop the polymer/mold assembly in an oven to achieve thermoformed micropatterned sTPE sheets while avoiding the need for a heat press.

2.1.2 | Self-sealing bonding strength

Fluoroflex microfluidic device assembly could be completed manually in a matter of minutes. Micropatterned sTPE sheets were cut to the desired size with scissors and holes were punched at the desired port locations with a steel hole punch. The sheets were then manually placed in conformal contact with pieces of un-patterned sTPE sheets of similar size, ensuring no air bubbles were present between the sTPE layers. Contact at this stage can easily be reversed and positioning of the sTPE layers can be adjusted. Robust self-sealing was achieved within minutes with simple conformal contact at room temperature, without baking. Assembled devices could optionally be baked at 185°C for 2 hours to achieve self-sealing with a stronger seal while still maintaining the structural and dimensional integrity of the molded parts.

This is markedly simpler than analogous procedures for glass and hard thermoplastic microfluidic devices, which require diverse and sometimes process-intensive and costly steps for sealing and interfacing.[45] Likewise, other fluoropolymer microfluidic devices reported in literature involve the use of adhesive layers[33,39] or thermal bonding[32,34] for sealing. Even PDMS, which can readily form conformal contact thanks to its elastomeric properties, requires plasma surface activation in order to achieve robust device sealing. Fluoroflex requires only conformal contact at room temperature for immediate device sealing, or optional baking for 2 hours. The sealing condition, with either room temperature or baking, was found to affect the bonding strength of Fluoroflex.

Self-sealing bonding strength was evaluated through pressure-regulated burst testing using a microfluidic device design consisting of two disconnected channels separated by a gap of 1 mm. The inlet channel was increasingly pressurized with water by a pressure controller in 50 mbar steps of 5 seconds each until delamination across the sTPE-bonded gap occurred, or until the maximum testing pressure of 4000 mbar was reached. Pressure testing was conducted on devices representing a variety of different sealing conditions following conformal contact in order to test the sealing pressure capacities achievable with and without baking measures. The first step in all sealing conditions was creating conformal contact between the two sTPE layers.

Pressure delamination tests showed bonded sTPE devices withstanding a maximum testing pressure of 4 bar after baking for 2 hours at 185°C. Room temperature sealing, consisting only of conformal contact between two sTPE layers, demonstrated time dependent strength. On shorter timescales (i.e., same-day production), microdevices sealed at room temperature for 5 minutes and 3 hours before pressure delamination testing showed bonding strengths of 1460 ± 22 and 1799 ± 229 mbar

(mean ± standard deviation), respectively. While the bonding strength of room temperature sealing is lower than that achieved by baking, if high pressure capacities are not required, it provides the possibility for near-immediate use of Fluoroflex devices after hot embossing (i.e., rapid prototyping). Room temperature sealing also eliminates the need for an oven, adding to the simplicity and accessibility of microfabrication with Fluoroflex. An additional set of delamination devices bonded at room temperature for 5 minutes exhibited a bonding strength of 1310 ± 96 mbar, showing little difference between batches of sTPE devices fabricated on different days. In comparison, the strength of PDMS-to-PDMS (irreversible) bonding via air or oxygen plasma surface activation commonly falls between 2 and 3 bar,[51,52] but has been reported in the range of 0.7–4 bar,[53] reflecting its high sensitivity to plasma parameters and environmental conditions. However, reversible sealing of PDMS to PDMS based on conformal contact at room temperature, similar to the sealing done with Fluoroflex, exhibits a bonding strength of approximately 0.4 bar.[51]

Room temperature sealing of Fluoroflex on longer timescales resisted higher pressures, with delamination devices withstanding 2350 ± 285 mbar 1 day after fabrication and 2850 ± 127 mbar 4 weeks after fabrication. The time dependence of sTPE bonding indicates a behavior similar to that of other sTPE materials. Lachaux et al., for example, described the Flexdym sTPE as a "slow adhesive polymer foil" for its intrinsic adhesive and cohesive properties resulting from the re-organization and interpenetration of mobile branched polymer chains at the interface of two polymer sheets.[40] This re-organization of polymer chains across the interface of two polymer sheets in conformal contact does not constitute covalent bonding between the two pieces. It occurs at room temperature and can be accelerated and enhanced with elevated temperatures (i.e., baking).

These findings highlight the potential for a streamlined fabrication methodology. Waiting a few days or weeks for robust room temperature bonding may be impractical in small-scale research contexts, especially when ovens are commonplace equipment. However, this material property could be particularly advantageous in larger-scale production, in which the removal of a processing step could have significant cost and logistical benefits when immediate bonding is not necessary. Bonding could, for example, take place in the transit time between a microdevice producer and a distributor or end-user.

The reversibility and reusability of Fluoroflex sealing was explored by testing sTPE devices re-bonded after already having been bonded. For example, two sets of delamination devices were sealed at room temperature and left for 1 day before being manually separated and immediately replaced in conformal contact. Delamination testing on the two sets was then conducted 5 minutes and 3 hours, respectively, after this second conformal contact was made. Resealing of Fluoroflex after an initial bonding and separation showed decreased bond strength. Delamination devices tested 5 minutes and 3 hours after resealing (at room temperature) exhibited bonding strengths of 990 ± 108 mbar and 1411 ± 273, respectively, both approximately 400 mbar inferior to the bonding strengths of their initial-bond counterparts, i.e., devices tested 5 minutes and 3 hours after their first sealing at room temperature. However, further loss of bonding strength was not found after additional separations and resealings. Devices separated and resealed at room temperature five times before delamination testing (5 minutes after the last resealing) exhibited a bonding strength of 1030 ± 76 mbar. Moreover, bonding strength could be recovered through baking. Baking for 2 hours at 185°C after separating and resealing five times at room temperature resulted in sTPE devices withstanding the maximum testing pressure of 4 bar. Similarly, devices that were sealed through baking, separated, and then baked again also withstood the maximum testing pressure of 4 bar.

Fluoroflex's reversible self-sealing opens new possibilities that are in contrast with the permanent bonding most often utilized with other microfluidic materials, be it PDMS, hard thermoplastics or glass. Reversible sealing provides a practical advantage of enabling the correction of manual errors or misalignments of multi-layered devices instead of discarding a flawed device. This also gives scope, for example, to separate and clean a device after use before being resealed and re-used, as well as the ability to fabricate modular devices, in which discrete functional device components can simply and quickly be mixed and matched with fast room temperature sealing. Modular microfluidics, leveraging Fluoroflex's self-sealing properties, is discussed further in Section 3.6.

Finally, to test the reusability of the sTPE material, one set of delamination devices was hot embossed using pieces of sTPE sheets that had already been hot embossed and bonded, instead of with raw sTPE pellets. These devices made from recycled Fluoroflex pieces showed a bonding strength of 1590 ± 129 mbar, incidentally slightly greater than the bonding strengths of the two sets of analogous devices fabricated with the same sealing conditions, but with raw sTPE pellets. These devices, made from recycled Fluoroflex, demonstrate the potential to reuse not only individual devices through reversible sealing, but also the material in its entirety through secondary hot embossing to fabricate new devices. This repurposing could translate to reduced material consumption, and with it, reduced cost

TABLE 1 Summary of self-sealing bond strengths of Fluoroflex after variable sealing conditions determined through delamination testing. sTPE delamination devices were sealed at either room temperature (RT) or 185°C and pressure tested after their first bond or after they had been separated and resealed (re-bond). Finally, one set (n = 5) of delamination devices was fabricated using recycled sTPE material that had already been hot embossed and bonded. Bond strengths are reported as mean ± standard deviation given a maximum testing pressure of 4000 mbar

Set No.		Sealing Condition	Bond Strength [mbar]
1	First bond, 185° C	2 h bake at 185° C, 1 h at RT	4000 ± 0 (max)
2	First bond, RT	5 min at RT	1460 ± 22
3	First bond, RT	5 min at RT (repeated set)	1310 ± 96
4	First bond, RT	3 h at RT	1799 ± 229
5	First bond, RT	1 day at RT	2350 ± 285
6	First bond, RT	4 weeks at RT	2850 ± 127
7	Re-bond, 185° C	2 h bake at 185° C, separation, 2 h bake at 185° C	4000 ± 0 (max)
8	Re-bond, RT	1 day at RT, separation, 5 min at RT	990 ± 108
9	Re-bond, RT	1 day at RT, separation, 3 h at RT	1411 ± 273
10	Re-bond, RT	1 day at RT, 5×(separation, 5 min at RT)	1030 ± 76
11	Re-bond, 185° C	1 day at RT, 5×(separation, 5 min at RT), 2 h bake at 185° C	4000 ± 0 (max)
12	Recycled sTPE, RT	Recycled sTPE hot embossing, 5 min at RT	1590 ± 129

for the end-user. A full list of bonding strengths of each of the different sTPE sealing conditions can be found in Table 1.

It is critical to note that while Fluoroflex can withstand pressures of 4 bar (and likely higher), due to its elastomeric properties (further discussed in Section 3.4) and the low thickness (approximately 700–1000 μm) of micropatterened sheets, some channel deformation and bulging occurred at the higher end of testing pressures. Thus, even if sTPE self-sealing withstands higher pressures, a stiffer material, such as glass, would be more suitable for applications requiring pressures above ~3 bar to maintain the integrity of channel geometry.

2.1.3 | Molding resolution

Optical profilometer measurements of micropatterned Fluoroflex sheets showed good molding resolution (Figure 1B). sTPE sheets preserved the features of the nickel-cobalt mold, reproducing the 70 × 70 μm channels to within 3 μm (4.3 %) difference in both channel height and width, likely due to minor thermal contraction after thermoforming inherent to thermoplastics.[54]

2.2 | Solvent compatibility

Investigating Fluoroflex's compatibility with common organic solvents is a critical step in determining its suitability as a flow chemistry microreactor material. Accordingly, a study of the effects of organic solvents on

hot-embossed sheets of the sTPE was conducted. The experimental procedure closely resembles that of Lee et al. in their study of PDMS solvent compatibility based on polymer swelling.[26] Micropatterned sTPE sheets were imaged before and after 24 hours exposure to a variety of common organic solvents. Pre and post-solvent exposure images were analyzed and polymer swelling was quantified by using a standard percent difference evaluation to define a "swelling ratio," $S = D_2/D_1$, where D_1 and D_2 are the measured polymer dimensions before and after solvent swelling, respectively. Post-solvent exposure images were captured while the samples were still immersed in order to avoid any potential de-swelling. A notable difference in experimental procedure from that of Lee et al. was the use of micropatterned polymer samples instead of simple, unpatterned polymer pieces. Measuring polymer dimensional changes with discrete, straight channels as references was found to be more precise than using sample edges as measurement references.

Fluoroflex swelling ratios show significantly less swelling than PDMS across the range of 26 solvents tested (Table 2).[26] Tetrahydrofuran (THF) (S = 1.43), 2-butanone (S = 1.44) and acetone (S = 1.43) caused the highest degrees of swelling in Fluoroflex. Polar aprotic solvents, including THF, 2-butanone, acetone, 1,2-dimethoxyethane and n-methylpyrrolidone, generally produced the strongest interactions observed, whereas polar protic solvents, such as alcohols and amines, and non-polar solvents, such as toluene, hexane and chloroform, produced little to no swelling effect in Fluoroflex.

Lee et al. considered PDMS "highly soluble" and generally incompatible with pure solvents at a swelling ratio

TABLE 2 Swelling ratios of Fluoroflex and PDMS (where, when D_1 and D_2 are the polymer dimensions before and after solvent swelling, respectively, the swelling ratio, $S = D_2/D_1$) for a selection of common organic solvents of solubility parameters, δ, in [joule$^{1/2}$ cm$^{-3/2}$].[55] Fluoroflex exhibits significantly less swelling than PDMS. PDMS swelling ratios from Lee et al.[26]

Solvent	δ	$S_{Fluoroflex}$	S_{PDMS}[1]
Pentane	14.5	1.00	1.44
Diisopropylamine	14.9	1.00	2.13
Hexane	14.9	1.00	1.35
n-Heptane	15.1	1.01	1.34
Triethylamine	15.3	1.00	1.58
Cyclohexane	16.8	1.00	1.33
1,2-Dimethoxyethane	18.0	1.27	1.32
Xylenes	18.2	1.00	1.41
Toluene	18.2	1.02	1.31
Benzene	18.8	1.00	1.28
Chloroform	18.8	1.01	1.39
Tetrahydrofuran	19.0	1.43	1.38
2-Butanone	19.0	1.44	1.21
Dimethylcarbonate	19.4	1.18	1.03
Chlorobenzene	19.4	1.00	1.22
Dichloromethane	20.3	1.03	1.22
Acetone	20.3	1.43	1.06
1,4-Dioxane	20.5	1.13	1.16
Pyridine	21.7	1.08	1.06
N-Methylpyrrolidone	22.7	1.27	1.03
Acetonitrile	24.3	1.08	1.01
1-Propanol	24.3	1.00	1.09
Dimethylformamide	24.8	1.22	1.02
Nitromethane	25.8	1.03	1.00
Ethanol	26.0	1.00	1.04
Methanol	29.7	1.01	1.02
Water	47.9	1.00	1.00

threshold of S = 1.28. Only three of the 26 solvents tested swelled Fluoroflex to this level, as compared to the 12 solvents that produced this effect in PDMS. With eight solvents still swelling Fluoroflex to a moderate degree (S ≥ 1.10), Fluoroflex's chemical compatibility is inferior to glass, which undoubtedly remains the material of choice when specific and extensive chemical resistances are sought. However, Fluoroflex exhibits greater chemical resistance than that of PDMS and other thermoplastics commonly used in microfluidic devices,[56] allowing a broader range of chemical reactions that could be performed in a polymeric device.

Solubility parameters are often used to estimate the interactions between polymers and solvents and have been vital in evaluating chemical compatibility of materials in lieu of empirical observation. The first single-component solubility parameter, introduced by Hildebrand and Scott,[57] is an expression of a material's cohesive energy density, whereby solubility (or polymer swelling in a solvent) in a two-phase system is maximized when the two solubility parameters are equal.[27] That is to say in this context, a solvent is more likely to swell or dissolve a polymer if their respective solubility parameters are close or equal to one another.

Fluoroflex's solubility parameter was calculated from the swelling data collected to estimate polymer-solvent interactions of solvents not tested. However, a single-component, Hildebrand solubility parameter model was found to be insufficient in describing the polymer-solvent interactions observed. For example, acetone and dichloromethane both have a Hildebrand solubility parameter of 20.2 joule$^{1/2}$ cm$^{-3/2}$, but acetone is one of the highest swelling solvents (S = 1.43) whereas dichloromethane swells Fluoroflex by only a minimal amount (S = 1.03). It is clear that a more descriptive model is necessary to describe the observed swelling behavior of Fluoroflex. Charles Hansen's three-component solubility parameter provided greater accuracy in describing solubility interactions, accounting for separate contributions of atomic dispersion forces, permanent dipole-dipole (polar) forces and hydrogen bonding to the overall cohesive energy density of a material.[55] The Hansen Solubility Parameter (HSP) thus consists of three components, δ_D (dispersion), δ_P (polar) and δ_H (hydrogen bonding), which can be resolved to a total solubility parameter, equivalent to the Hildebrand solubility parameter, δ, through the relationship, $\delta^2 = \delta_D^2 + \delta_P^2 + \delta_H^2$. The three-component HSP can be understood as a point in a three-dimensional solubility space with a solubility radius, R_O. A solvent having an HSP that falls within the HSP sphere of another material is then expected to produce a solubility interaction, whether it be miscibility in liquid-liquid cases or dissolution/swelling in solid-liquid cases.

Iterative fitting (Data Fit of 1.00) of an HSP resulted in an estimated Fluoroflex HSP of δ = 21.2 joule$^{1/2}$ cm$^{-3/2}$, consisting of components δ_D = 16.5, δ_P = 8.9 and δ_H = 9.7 joule$^{1/2}$ cm$^{-3/2}$, with a sphere radius of R_o = 7.5 joule$^{1/2}$ cm$^{-3/2}$ (Figure 2). The HSP fit containing the smallest radius of interaction, R_O, was deemed superior and is presented above. However, it must be noted that given the solvent swelling data set size, room for minor variation in the final HSP exists while still maintaining a Data Fit of 1.00. These nuances in HSP data fitting, further discussed in the supporting information (including Figure S2), underscore the inherent difficulties of solubility parameter estimations, particularly in the border regions of solubility spheres[58] and when polymer swelling, as opposed to dissolution, is concerned.[59]
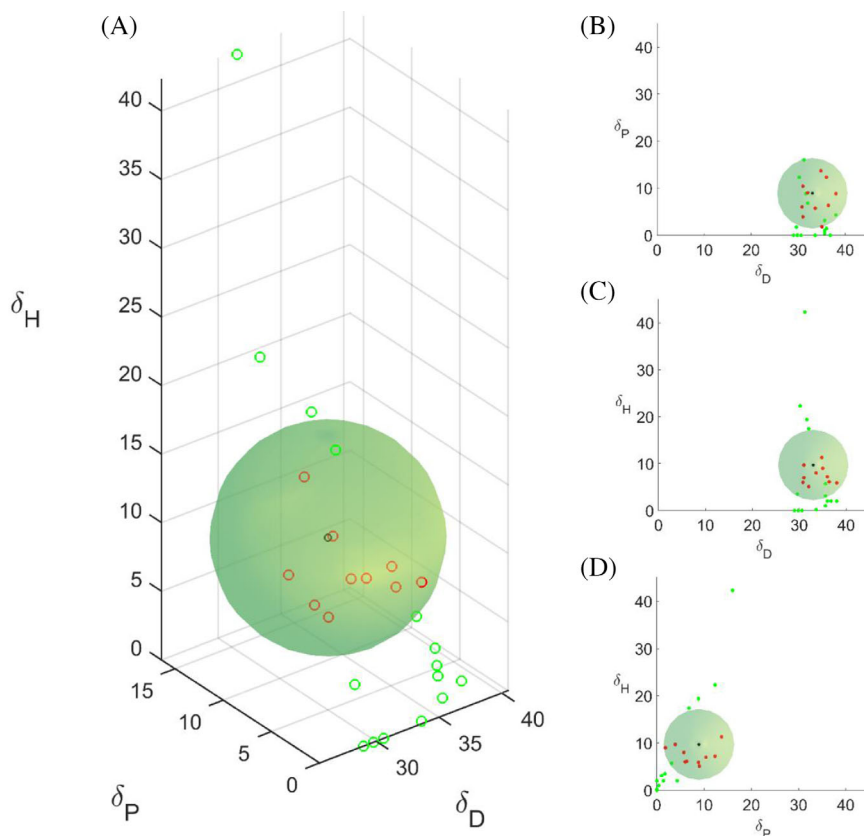
FIGURE 2 Hansen solubility parameter estimation for Fluoroflex based on polymer solvent swelling data from Table 1: $\delta_D = 16.5$, $\delta_P = 8.9$ and $\delta_H = 9.7$ joule$^{1/2}$ cm$^{-3/2}$, with a sphere radius of $R_O = 7.5$ joule$^{1/2}$ cm$^{-3/2}$. A, HSP sphere of Fluoroflex with center (black) in a solubility "space," having dispersion, polar and hydrogen bonding dimensions. Red points represent solvents having some swelling effect (S > 1.02) on Fluoroflex, while green points represent those producing no or negligible swelling. B-D, HSP sphere with HSP components shown pair-wise for ease of viewing. Note that a scaling factor of two is used for the dispersion component, δ_D, for effective graphical representation of a spherical HSP, as described by Hansen.[55] Graphs in units of [joule$^{1/2}$ cm$^{-3/2}$]

This HSP should thus be used conservatively as a tool by a potential user of Fluoroflex if using a solvent not included in this work, or indeed a solvent mixture that exhibits a certain HSP. Solvent blending, informed by Fluoroflex's HSP, could moreover be a means of mitigating the adverse effects of the few solvents that have high swelling effects on Fluoroflex.

2.3 | Optical properties

Optical characterization of Fluoroflex was an important step in understanding its suitability for a variety of microfluidic applications, particularly where imaging and irradiation (e.g., photocatalysis on-chip) are necessary.

2.3.1 | UV-Vis spectroscopy

UV-Vis measurements on Fluoroflex sheets showed high optical transparency of the material into the near UV range, with over 50% transmission down to 334 nm (Figure 3A). This optical transparency is comparable or superior to other thermoplastics used for microfluidics, such as PMMA[60] and PC,[61] and would allow observation and imaging with a range of fluorescent dyes. Both UV irradiation and exposure to acetone (24 hours exposure for sTPE

swelling, followed by 24 hours de-swelling in air) showed little effect on the optical transmission of the sTPE.

2.3.2 | Autofluorescence

Like some other thermoplastics used for microfluidics,[62] Fluoroflex was found to exhibit autofluorescence. Fluorescence mapping revealed peak autofluorescence at an excitation wavelength of 370 nm (Figure 3B). This poses limitations of the material for fluorescent imaging, particularly with excitation wavelengths in the violet and UV ranges. Depending on the given application, this needs to be considered when using Fluoroflex microfluidic devices.

2.3.3 | Refractive index

The refractive index of a microfluidic device can be an important property when choosing an optical imaging setup to optimize resolution and clarity.[63,64] Fluoroflex was found to have a refractive index of n = 1.36. Its low refractive index compared to glass (n = 1.46) and PDMS (n = 1.41),[65] in addition to its similarity to the refractive index of water (n = 1.33), could be advantageous in applications involving imaging in aqueous media or with water-immersion objectives.
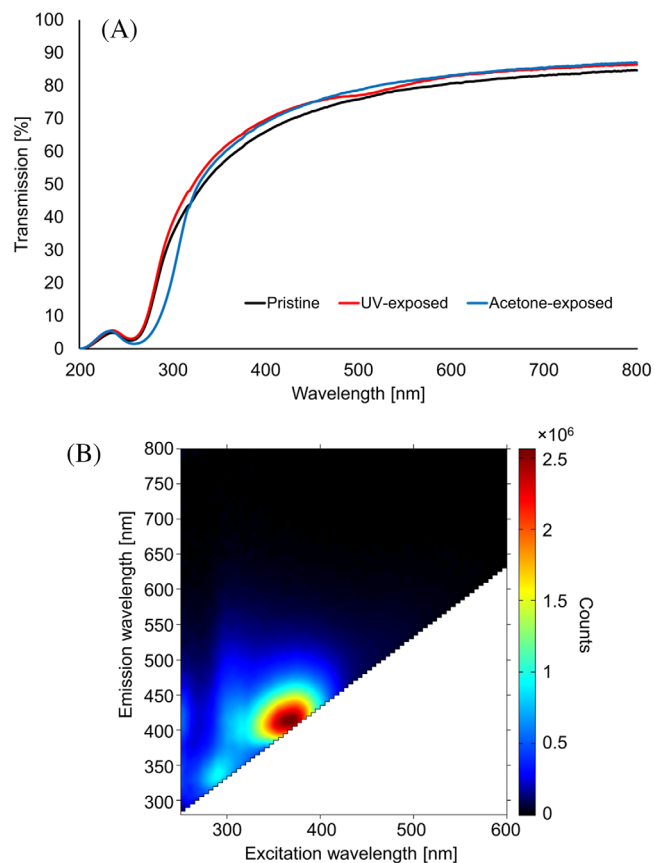
FIGURE 3 A, UV-Vis spectra of Fluoroflex samples, 1 mm in thickness, exhibiting high optical transmission into the near UV wavelengths. Exposure of sTPE sample to UV light and acetone swelling had negligible effect on transmission. B, Fluorescence mapping of Fluoroflex, showing autofluorescence in the UV and violet excitation wavelengths with a peak at 370 nm

2.3.4 | FTIR spectroscopy

While solvent swelling and UV (365 nm) exposure had no apparent permanent effect on Fluoroflex samples, these conditions can cause unseen degrading effects on polymers.[66,67] To this end, FTIR measurements were conducted to investigate any structural changes that could occur in Fluoroflex as a result of material swelling and UV exposure. FTIR spectra showed no significant changes across the range of UV and acetone-exposed samples (Figure S3), suggesting no material structural alterations occurred as a result of these conditions.

2.4 | Mechanical and surface properties

2.4.1 | Tensile testing

Basic mechanical testing was performed on Fluoroflex to determine general mechanical behavior and quantify the

elastomeric properties that can be important in informing material fabrication and deformability. In tensile strength testing (from 0% strain to specimen rupture), the material shows two different regions of deformation (Figure 4A). The change in behavior takes place between approximately 40% and 70% strain, beyond which the material exhibits lower stiffness. Tensile strength analysis focused on strain levels under 20%, as high levels of strain are not expected during the use of Fluoroflex as a microfluidic device. For this range of deformation, the mechanical behavior of this material is not entirely linear elastic, with decreased stiffness at higher strain levels, resulting in a mean elastic modulus of 4.75 ± 0.22 MPa and 3.75 ± 0.17 MPa (mean ± standard deviation; n = 10) for strains of $\epsilon < 5\%$ and $\epsilon < 20\%$, respectively (Figure 4B). This tensile stiffness is the same order of magnitude as that of PDMS, which is most often in the range of ~1–3 MPa.[68–70] This relatively low stiffness eases demolding and is critical for reliably creating conformal contact between sTPE layers for bonding, in contrast with hard thermoplastics, having stiffness in the order of giga pascals.[46] Fluoroflex samples were taken to rupture and exhibited 434% ± 44% elongation at break.

2.4.2 | Surface wetting

Contact angle measurements were made to understand the solid-liquid surface behavior of Fluoroflex. Surface wetting properties can be imperative in anticipating and manipulating precision microfluidic flow control,[71] particularly in multiphase flow.[72–75] Goniometer measurements of water and diiodomethane on Fluoroflex sheets showed hydrophobic surface behavior of Fluoroflex ($\theta_{Water} = 105.0 \pm 1.2°$, $\theta_{Diiodomethane} = 64.9 \pm 0.7°$; n = 5) (Figure S4a–b). Exposure of samples to acetone prior to contact angle measurements had negligible effect on the sTPE surface wetting properties ($\theta_{Water} = 105.1 \pm 0.8°$, $\theta_{Diiodomethane} = 64.6 \pm 1.3°$; n = 5). The two-component surface energy of Fluoroflex was determined through the Fowkes method [76] to be purely dispersive ($\sigma_{Fluoroflex} = 25.6$ mJ m^{-2}). This wetting behavior and low surface energy characteristics are close to those of PDMS.[77] This could permit the use of well-documented PDMS surface wetting behavior as an analog to inform and evaluate microfluidic flow in Fluoroflex devices.

2.4.3 | Surface roughness

Atomic force microscopy (AFM) surface roughness evaluations of Fluoroflex revealed that pristine sTPE sheets hot embossed between silicon wafers (wafer roughness
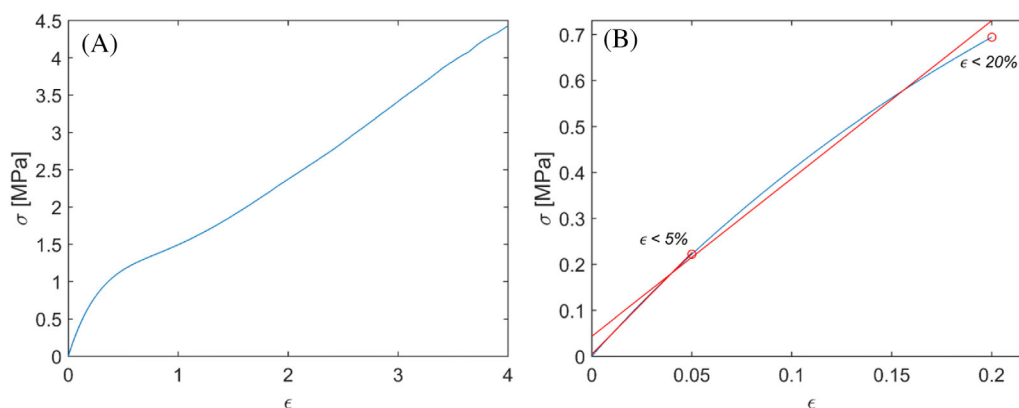
FIGURE 4 A, The tensile stress-strain curve of a Fluoroflex sample taken to rupture at ~450% strain, showing two distinct regions of stiffness. Higher stiffness was measured in strains up to ~40% before a transition to lower stiffness above ~70% strain. B, Zoom of the Fluoroflex stress-strain curve for a strain of 0%–20%, with linear fits for $\epsilon < 5\%$ and $\epsilon < 20\%$ (both in red) approximating the mean tensile modulus for these strain ranges

$R_{RMS} = 1.6 \pm 1.0$ nm; mean $\pm$ standard deviation, n = 9 images of one wafer) had a roughness of $R_{RMS} = 5.7 \pm 3.1$ nm (n = 20 images, two sTPE sheets). Swelling and subsequent de-swelling of Fluoroflex in acetone showed a statistically insignificant effect on surface roughness ($R_{RMS} = 4.3 \pm 2.0$ nm; n = 19 images, two sTPE sheets; ANOVA: $F(1, 37) = 3.07$, $P = 0.09$), with no evidence of surface cracking or degradation after material swelling. It must be noted that sTPE sample microfabrication was not conducted in a cleanroom, thus a slight decrease in sTPE surface roughness after acetone exposure could be the result of the cleaning effects of solvent submersion on surface contaminants. An important contribution in the total roughness comes from isolated defects, such as hills or pits, in the sTPE sheets. In defect-free regions the roughness can be as low as $R_{RMS} = 1.6$ nm, which can be considered as a lower limit for the surface roughness of Fluoroflex sheets. The surface roughness achievable with Fluoroflex is sufficiently low (< 1% relative roughness) as to be considered smooth on a microfluidic scale, having a negligible effect on flow resistance.[78–80] A surface roughness of 5.7 nm in a 50 μm (diameter or width and height) microfluidic channel, for example, represents a relative roughness of ~0.01%. Maintaining low surface roughness in microfluidics also has broader implications in facilitating reliable device bonding[47,81,82] and high optical clarity[83,84] in thermoplastics. Roughness analyses suggest that the limiting factor in achieving good molding reproduction of surface topography with surface roughness below 10 nm would depend on the roughness of the master mold and not on any roughness inherent to the material itself or resulting from the hot embossing process. AFM topography images can be found in Figure S4c–f.

2.5 | Absorption and oxygen permeability

2.5.1 | Small molecule absorption

PDMS has been well documented in absorbing a variety of drug and dye compounds, which can have a significant impact on experimental outcomes.[85] For an evaluation of small molecule absorption of Fluoroflex, a rhodamine B absorption assay was conducted to compare the sTPE to PDMS in this respect. Fluoroflex and PDMS microchannels were filled with an aqueous rhodamine B solution and left to incubate for 24 hours at room temperature before being imaged with a fluorescent microscope. The channels were then thoroughly rinsed with DI water before being imaged again. In comparison to PDMS, Fluoroflex exhibited minimal residual fluorescence after rinsing, and no observable absorption into the bulk of the material through the channel walls (Figure 5), a favorable property for applications as a microreactor.

2.5.2 | Oxygen permeability

The presence of oxygen, or lack thereof, can be a critical factor in both biological and chemical experimentation.[86,87] Thus, quantifying the degree to which a given material permits the flux of oxygen from ambient air into a sealed microfluidic channel is of high importance. The oxygen permeability of Fluoroflex was found to be 4.04 ± 0.79 Barrer (mean $\pm$ standard deviation) compared to a permeability of 563.5 ± 12.1 Barrer of PDMS. The oxygen permeability of PDMS found experimentally is on the lower end of values reported in

FIGURE 5 Rhodamine B absorption analysis in PDMS and Fluoroflex microchannels measuring 400 μm (width) x 55 μm (height). Fluorescent images of (A) PDMS and (B) Fluoroflex channels containing 100 μM Rhodamine B in water after 24 hours incubation. Images (C) and (D) show the same PDMS and Fluoroflex channels, respectively, after rinsing with DI water with corresponding fluorescence intensity line profiles across the PDMS (E) and Fluoroflex (F) channels, where the black and red lines correspond to the normalized intensity of the channels pre and post rinsing, respectively
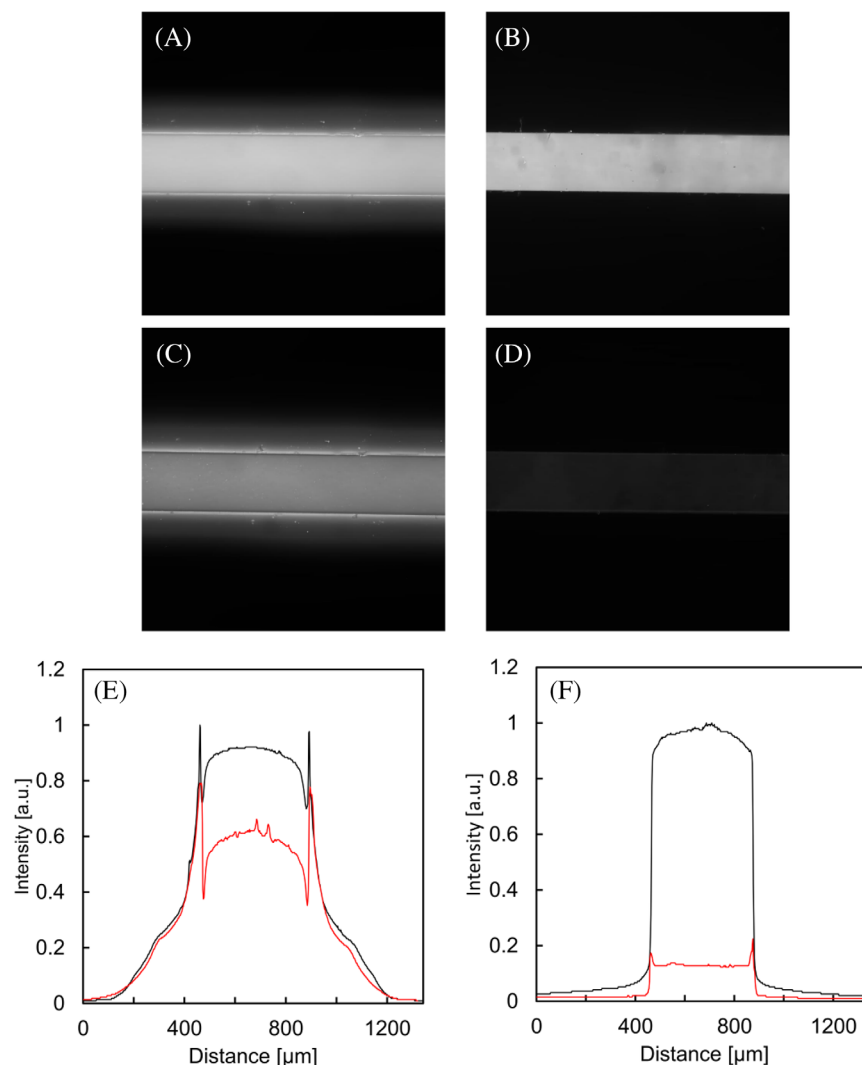
literature,[88,89] but still represents an oxygen permeability more than two orders of magnitude greater than that of Fluoroflex. As compared to PDMS, this provides greater opportunity for the sTPE to be used as a microreactor for oxygen-sensitive chemical reactions or where oxygen concentrations or gradients on-chip must be controlled.

2.6 | Modular droplet generation

The fast, room temperature self-sealing property of Fluoroflex enables the use of sealed microdevices mere minutes after assembly. At the same time, the reversibility of the bonding allows for the removal, adjustment and reuse of individual sTPE pieces. By leveraging these characteristics, devices can be easily configured and reconfigured by combining discrete microfluidic components, or modules. To this end, a modular sTPE device for droplet generation was fabricated to demonstrate the simplicity and utility of device modification thanks to fast self-sealing. The mod-

ular device consisted of a hot-embossed sTPE baseplate, or manifold, containing designated spaces on its surface to host individual microfluidic modules. Holes punched in one layer of the baseplate allowed fluid connections between modules and the device inlets and outlets through a simple network of sealed channels (Figure S5).

The modular device initially contained two micropatterned modules: a simple straight channel and a T-junction droplet generator, both bonded at room temperature to the surface of the baseplate (Figure 6A). Water was pumped through the straight channel (250 μm width) to the 100 μm T-junction, where droplets of approximately 90 μm in diameter were formed in a continuous phase of toluene (Figure 6B). The sTPE exhibited no deformation or leaking caused by the toluene, a solvent that readily swells PDMS. The T-junction module was then manually removed and a larger T-junction module (250 μm) was put in its place (Figure 6C). Within minutes, droplets of approximately 140 μm were generated with the new T-junction module without altering any other fluidic connections or pressure
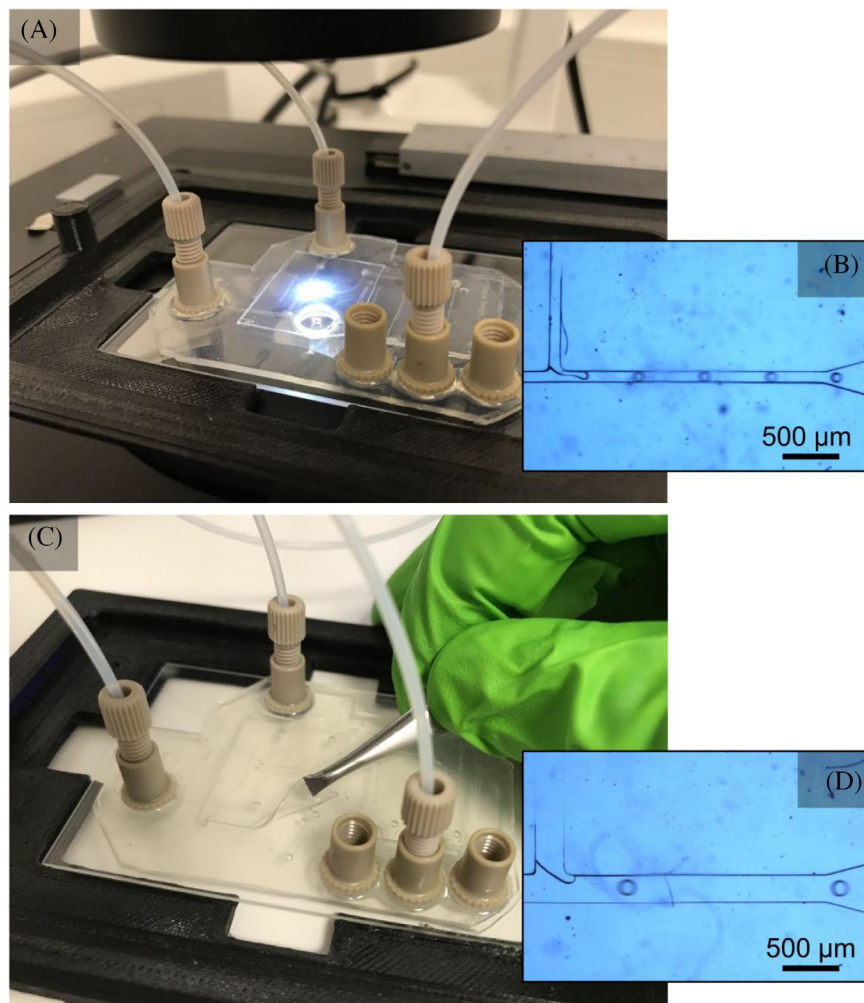
FIGURE 6 Modular microfluidic device based on sTPE room temperature self-sealing. A, Modular sTPE device consisting of an sTPE baseplate and two microfluidic modules (a straight channel, right, and a T-junction droplet generator, left) bonded to the surface of the baseplate. Connectors were fixed to the baseplate with UV curing glue to allow microfluidic tubing interfacing. Using a 100 µm T-junction first, water droplets of approximately 90 µm were generated in a continuous phase of toluene (B). The 100 µm T-junction module was then removed with tweezers (C) and replaced with a larger, 250 µm T-junction module, with which droplets of approximately 140 µm were generated (D). Reconfiguration of the device with the second T-junction module was completed in a matter of minutes thanks to the fast and reversible room temperature self-sealing of Fluoroflex

control settings (Figure 6D). Next, the straight channel was replaced with a co-flow Y-channel module, allowing the droplet phase to contain the mixture of two fluids instead of one. To demonstrate this, fluorescent droplets were generated using an aqueous rhodamine B solution (100 mM) from one inlet and pure DI water from the second inlet (Figure S5f-h). Other conceivable adjustments would be adding a subsequent module in series, downstream of the droplet generation to increase residence time for droplet viewing, mixing, etc. Extensions of increasingly complex liquid manipulation, with or without droplets, becomes possible by considering a wide variety of modules. The only constraint for the modules is that they are designed to fit the dimensions of the baseplate fluid connections. Accordingly, the quick self-sealing properties of Fluoroflex would permit true "plug-and-play" operation, effective for rapid prototyping and device optimization – similar to electronic bread boards.

In combination with Fluoroflex's straightforward and transferrable thermoplastic fabrication method, a modular device platform gives scope for the development of the large-scale industrialization of standardized microfluidic

devices both in terms of device production and ease of use.[90]

3 | CONCLUSION

This study introduces a new fluorinated soft thermoplastic elastomer, Fluoroflex. The sTPE can be micropatterned in 30 seconds with high fidelity by hot embossing using standard microfluidic molds. Fluoroflex exhibits a spontaneous cohesive property upon conformal contact, allowing it to be simply sealed to itself at room temperature or with baking measures in order to assemble closed-channel microfluidic devices. This self-sealing eliminates the need for plasma surface activation, adhesives or other process-intensive bonding procedures commonly used to seal microdevices. The resulting sTPE self-bonding is reversible and can withstand pressures up to ~2.8 bar with room temperature sealing and at least 4 bar with baking, determined through pressure delamination testing. Its room temperature bonding strength was found to increase with time, even after achieving a bonding strength of ~1.4 bar after

only 5 minutes. The ease of sTPE device fabrication and material recyclability sharply contrasts with device microfabrication using other common materials, and lends heavily to its accessibility and scope for transferability across manufacturing scales. This is a critical consideration with respect to potential device commercialization and industrial implementation.[91]

Fluoroflex's solvent compatibility was determined to exhibit good solvent resistance to a range of common organic solvents. While falling short of the solvent resistance of glass or pure PTFE, it represents a marked improvement over other polymeric materials used for microfluidics, such as PDMS, PC and PMMA. In addition to more comprehensive solvent resistance, glass would also be more suitable for high pressure/high temperature applications.

We also characterized a range of Fluoroflex's material properties pertinent to its use as a microreactor. Namely, it was found to be optically transparent down to the near-UV range, have hydrophobic surface behavior, low surface roughness (~5 nm), oxygen gas permeability two orders of magnitude lower than that of PDMS and a mean elastic modulus of 3.75 MPa ($\epsilon < 20\%$).

Finally, droplet generation was conducted in a Fluoroflex device to demonstrate the use of an organic solvent in a precision microfluidic context. The device showcased the fast, reversible self-sealing of the sTPE, allowing for discrete microfluidic components to be interchanged in a "modular" system. Combined with the ease and accessibility of device fabrication, this could allow for rapid prototyping or "plug-and-play" functionality of chemical microreactors.

To our knowledge, this is the first fluorinated thermoplastic that can be rapidly micropatterned and exhibits self-sealing upon conformal contact. We believe it represents a combination of material properties and processing simplicity of broad interest to the microfluidics and flow chemistry communities.

4 | EXPERIMENTAL METHODS

4.1 | sTPE hot embossing and sealing

The nickel-cobalt master mold (Eden Tech SAS, Paris, France) contained a network of serpentine channels (70 μm width, 1:1 aspect ratio). The dry film photoresist molds contained various microchannel designs and were fabricated using Ordyl SY 300 dry film negative photoresist (55 μm thickness, ElgaEurope s.r.l., Milan, Italy) laminated on 75 × 50 mm borosilicate glass slides (Corning Inc., Corning, USA) as described previously.[92] sTPE hot embossing was performed with a DC8 manual heat press (Geo Knight

& Co Inc., Brockton, MA, USA). Both the top and bottom heated plates of the press were heated to 220°C before placing the mold-sTPE-counter-plate assembly on the lower heated plate. The upper heated plate was brought into contact with the assembly and was left for 15 seconds to heat the assembly under no supplementary pressure. Approximately 5 bar of pressure was applied to the assembly via the lever arm of the upper heated plate. Sealing of sTPE devices by baking was conducted in a DKN612C forced convection oven (Yamoto Scientific Co. Ltd., Tokyo, Japan).

4.2 | Delamination testing

The inlet of the delamination devices was interfaced with a microfluidic circuit via PTFE tubing (1/16″ OD, 1/32″ ID) using a compression-based chip holder (Eden Tech SAS, Paris, France). The pressure sequence was implemented using an OB1 MK3+ pressure controller (0–8000 ± 0.5 mbar, Elveflow, Elvesys SAS, Paris, France). Delamination of the 1 mm gap bond was accompanied by the flow of water from the previously dead-end inlet channel across the gap and into the device's outlet channel before exiting the device entirely via the second punched hole. Accordingly, an in-line flow sensor (MFS3, -80–80 μL min^{-1} ± 5% m.v., Elveflow, Elvesys SAS, Paris, France) was used to determine the precise moment at which delamination occurred (indicated by a non-zero flow rate). A more detailed description of the delamination device design and a similar pressure testing setup has been previously described.[92] Pressure testing was conducted on devices in sets of n = 5 devices.

4.3 | Optical profilometry

Measurements were done using a Wyko NT9100 (Veeco Instruments Inc., Plainview, NY, USA) on sTPE sheets patterned with serpentine microchannels using the nickel-cobalt master mold described above. Measurements were also taken of the master mold itself for comparison.

4.4 | Solvent testing

The above-described nickel-cobalt master mold was used to hot emboss sTPE sheets of approximately 1 mm thickness with channels of 70 μm width and depth, which were then cut with scissors into discrete pieces. Micropatterned sTPE pieces were imaged using a stereoscope (Leica DMS300, Leica Microsystems Inc., Buffalo Grove, IL, USA) and the orthogonal distances between the parallel microchannels edges on each piece were measured

through image analysis (FIJI[93]). After imaging, the sTPE pieces were placed in containers of 26 common organic solvents (standard laboratory grade ≥ 95%, Sigma-Aldrich, St, Louis, MO, USA) and water (n = 5 pieces per solvent) and left at room temperature for 24 hours under complete immersion. Each piece was subsequently reimaged while remaining immersed in the solvent, and the distances between the microchannels were again measured through image analysis. The pre solvent-exposure dimensions measured were approximately 6.6 mm on the polymer sheets, and post solvent-exposure distances varied depending on the level of swelling exhibited by the polymer. PDMS samples (SYLGARD 184, Dow Inc., Midland, MI, USA) were prepared and tested in the same manner with a few solvents to validate the coherence of swelling data in literature with swelling data obtained through this experimental method.

Fitting of a Hansen Solubility Parameter (HSP) for Fluoroflex followed the standard iterative method developed by Charles Hansen.[55] Solvents were designated as "swelling" (S > 1.02) and "non-swelling" solvents based on solvent swelling observations. An initial estimate of the HSP of Fluoroflex with radius, R_O, was made based on the average HSP values of all the swelling solvents. A quality-of-fit was evaluated based on the location of the swelling and non-swelling solvent HSPs in relation to the polymer HSP solubility sphere initial estimate, whereby an error in the fit was denoted by a swelling solvent falling outside of the estimated HSP sphere or a non-swelling solvents falling inside of the sphere. More specifically, the error value is equal to the distance between the erroneous solvent and the edge of the HSP sphere. That is,

$$ERROR\ DISTANCE = R_o - R_a \tag{1}$$

For non-swelling solvents inside the estimated sphere and,

$$ERROR\ DISTANCE = R_a - R_o \tag{2}$$

For swelling solvents outside of the estimated sphere, where R_a denotes the distance between the sphere center, $(\delta_{D1}, \delta_{P1}, \delta_{H1})$, and a given solvent's HSP, $(\delta_{D2}, \delta_{P2}, \delta_{H2})$, from literature:[55]

$$R_a = \sqrt{4(\delta_{D2} - \delta_{D1})^2 + (\delta_{P2} - \delta_{P1})^2 + (\delta_{H2} - \delta_{H1})^2} \tag{3}$$

The constant, 4, in the equation was found to be appropriate in representing solubility data as a sphere.[55] The method uses a quality-of-fit function called the "Desirability Function,"[94] where the data fit is calculated as,

$$Data\ Fit = (A_1 * A_2 * ... * A_n)^{1/n} \tag{4}$$

When,

$$A_i = e^{-(ERROR\ DISTANCE)} \tag{5}$$

Swelling solvents falling inside of the sphere, as well as non-swelling solvents falling outside of the sphere, contributed to a Data Fit of 1.00 (no error), with fitting iterations aimed at optimizing this case given the experimental swelling data recorded. Subsequent iterations of Fluoroflex's three HSP components and R_O were performed in order to maximize the data fit toward 1.00.

4.5 | Optical characterization

All optical characterization was performed on sheets of pristine, un-patterned Fluoroflex hot embossed between two silicon wafers (University Wafer Inc., South Boston, MA, USA). Sheets of 1.5 mm thickness were cut with scissors to the desired sample size for each of the following optical characterization procedures.

4.6 | UV-vis spectroscopy

Absorption spectra (200–800 nm) of pristine sTPE samples were measured with a Lambda 950 spectrophotometer (PerkinElmer Inc., Waltham, MA, USA). A second set of UV-Vis measurements were performed on samples that had been exposed to UV light (365 nm; 70 mW cm^{-2} for 8 hours, or 2016 J cm^{-2}) using a UV Chamber (UWAVE, Les Ulis, France). A positive control for swelling was evaluated to determined shifts in spectra post-swelling. Fluoroflex samples were immersed in acetone for 24 hours at room temperature, and then allowed to de-swell for 24 hours prior to measurements being taken.

4.7 | Refractometry

The refractive index of pristine Fluoroflex samples was measured with an Abbe 5 refractometer (Bellingham + Stanley Ltd., Kent, UK).

4.8 | Fluorescence spectroscopy

Autofluorescence measurements (λ_{exc} = 250–600 nm; λ_{em} = [λ_{exc}+30]–800 nm) were conducted on pristine Fluoroflex samples using an Edinburgh FLS908 spectrometer (Edinburgh Instruments Ltd., Livingston, UK). A MATLAB script (The MathWorks, Inc., Natick, Massachusetts, USA) was used to plot an autofluorescence

excitation/emission heat map across the range of wavelengths tested.

4.9 | FTIR spectroscopy

Transmission measurements were performed on solid pristine Fluoroflex samples (in the range of 4000–400 cm^{-1} using a Nicolet iS 5 FTIR spectrometer (Thermo Fisher Scientific, Waltham, MA, USA). The FTIR spectra were compared to those measured of both UV-exposed (1, 2, 4 and 8 hours exposure time) and acetone-exposed samples investigate the effect of UV irradiation and solvent swelling on the material composition.

4.10 | Tensile testing

Mechanical characterization consisted of uniaxial tensile tests. All tests were performed with an INSTRON 5848 microtester (INSTRON, Norwood, MA, USA). Dog-bone samples of approximately 20 mm length and 2 × 2 mm cross section were fabricated by pressing sTPE pellets into laser-cut stainless-steel molds using the same hot embossing parameters as described above. A controlled traction displacement of 1 mm min^{-1} was applied (from 0 to specimen rupture). In the range of interest (0%–20% strain), no reduction in the cross-sectional area of the specimen was assumed to calculate stress and subsequent elastic modulus using Hooke's law. The test was performed in ten different specimens of 19.73 ± 1.65 mm in length (mean ± standard deviation) and 2 × 2 mm cross-section.

4.11 | Contact angle

Measurements were performed using the pendant drop method. Water and diiodomethane droplets were dispensed onto the surface of pristine sTPE sheets hot embossed between two silicon wafers, as well as onto acetone-exposed sTPE sheets. The droplets were imaged and analyzed using a CAM 200 contact angle goniometer (KSV Instruments, Helsinki, Finland).

4.12 | Atomic force microscopy

Fluoroflex sheets of 1 mm thickness were hot embossed between two silicon wafers and topographic images of 6 × 6 μm, 4 × 4 μm and 2 × 2 μm of the sheets were recorded in tapping mode with a PicoSPM 5100 scanning probe microscope (Agilent Technologies, Santa Clara, CA, USA). Additional imaging was performed on sTPE sheets after acetone swelling and de-swelling, as well as one of the silicon wafers used for hot embossing. Measurements were taken in ambient conditions using silicon cantilevers (AC160TS-R3, Olympus Corporation, Tokyo, Japan) with resonance frequency around 300 kHz and spring constant around 26 N m^{-1}, and subsequent roughness analyses were conducted with WSxM 5.0 software.[95] A one-way analysis of variance (ANOVA) was conducted to evaluate statistically significant variation in surface roughness between pristine and acetone-swelled sTPE samples, where variation was considered significant when $P < 0.05$.

4.13 | Rhodamine B absorption

Microfluidic devices consisting of a simple channel of 400 μm width and 55 μm height were fabricated in Fluoroflex using an Ordyl master mold and the hot embossing and self-sealing procedure described above. The same mold was used to fabricate PDMS devices. Liquid PDMS base (SYLGARD184, Dow Inc., Midland, MI, USA) was mixed with crosslinker at a ratio of 10:1 (base:crosslinker) then degassed under vacuum for 20 minutes. The mixture was poured atop the master mold and baked at 80°C for 2 hours. PDMS devices were removed from the mold and cut, then 1.5 mm holes were punched with a biopsy punch at device inlets and outlets. Devices were bonded to borosilicate glass microscope slides (76 x 26 mm, 1 mm thickness, Thermo Fisher Scientific, Waltham, MA, USA) by making conformal contact with the PDMS surface after plasma treatment with a plasma cleaner (PDC-002, 200 mTorr, 30 W, 2 minutes, Harrick Plasma, Ithaca, NY, USA). Devices were left on a hot plate at 120°C for 30 minutes to complete the fabrication process. Rhodamine B dye (100 μM in water, Sigma-Aldrich, St. Louis, MO, USA) was loaded by syringe into both a Fluoroflex and PDMS channel and left to incubate in ambient conditions for 24 hours. Devices were then imaged with a fluorescent microscope (Zeiss Axio Observer Z1, Carl Zeiss AG, Oberkochen, Germany) and subsequently flushed continuously with DI water for 10 minutes, after which devices were re-imaged. Images were analyzed using FIJI.[93]

4.14 | Oxygen permeability

Fluoroflex films of approximately 200 μm thickness were fabricated by hot embossing sTPE pellets between two metal plates for 30 seconds. PDMS films (SYLGARD 184, 10:1 [base:crosslinker]) of approximately 115 μm thickness were spin coated using an initial 10-second step at 500 rpm and a subsequent 30-second step at 800 rpm with 300 rpm s^{-1} acceleration (Spin 150 spin coater, SPS-Europe B.V.,

Putten, The Netherlands) followed by baking for 2 hours at 80°C. The oxygen pure gas permeability of Fluoroflex and PDMS films was measured using a custom-made high-throughput gas separation (HTGS) setup, as previously described.[96–98] The active membrane permeation area was 1.91 cm^2 per coupon. A constant-volume-varying-pressure method was applied to determine the oxygen permeability. Permeate gas was accumulated in a 75 cm^3 measuring cylinder and the change in pressure inside the cylinder was monitored by a pressure sensor (MKS Baratron, MKS Instruments, Munich, Germany) as a function of time (dp/dt). Permeability of the gas is then calculated with equation 6:

$$P_{O_2} = 10^{10} \times \frac{V \times V_m \times L}{p_{up} \times A \times R \times T} \times \frac{dp}{dt} \qquad (6)$$

where P_{O_2} is the oxygen gas permeability (Barrer), V is the downstream volume (75 cm^3), V_m is the molar volume (22.414 L mol^{-1}), A is the membrane permeation area (1.91 cm^2), L is the membrane thickness (µm), T is the operating temperature (K), p_{up} is the upstream pressure (bar), R is the gas constant (0.082 L atm mol^{-1} K) and dp/dt is the pressure change (Torr s^{-1}). Permeability measurements were conducted at 6 bar feed pressure and 35°C.

4.15 | Modular droplet generation

All sTPE sheets were hot embossed using the same parameters as above (220°C for 30 seconds) using molds made from Ordyl dry film photoresist on glass slides. The baseplate (approximately 75 × 25 mm in size) consisted of one sTPE sheet hot embossed with channels measuring 110 × 500 µm (height × width) bonded to a featureless sTPE sheet. Holes were punched in the micropatterned sheet at the ends of each of the channels for tubing interfacing and fluid connections between modules. PEEK NanoPort assemblies, including perfluoroelastomer (FFKM) gaskets (N-333, Darwin Microfluidics, Paris, France), were fixed to the top of the baseplate with Loctite 3106 UV curing glue (CureUV, Delray Beach, FL, USA), cured with 30 seconds of UV exposure using a Scangrip UV-PEN (25 mW cm^{-2}, 390–400 nm; SCANGRIP North America Inc., Atlanta, GA, USA). Individual modules (17 × 25 mm) were placed in conformal contact with the baseplate top surface in alignment with the appropriate baseplate channels and holes for bonding at room temperature. All modules had channels 110 µm in height. 1/16″ OD PTFE tubing was used to interface the modular device with reservoirs of deionized water and toluene (≥ 95%, Sigma-Aldrich, St, Louis, MO, USA), pumped using an OB1 MK3+ pressure controller (0–2000 ± 0.1 mbar, Elveflow, Elvesys SAS, Paris,

France). Droplet generation was imaged using a Pixelink PL-D725CU camera (Pixelink, Ottawa, Canada) on a Zeiss Axio Observer Z1 microscope (Carl Zeiss AG, Oberkochen, Germany) and images were analyzed using FIJI.[93]

CONFLICT OF INTEREST

The authors A.H.M. and S.C.L.P., at the time of this work, were employees of Elvesys SAS, a company that sells Elveflow equipment, which was used for flow control and measurements in this work. E.R. is the co-founder and CEO of Eden Tech, which commercializes polymers for microfluidics. I.O. is a promoter and consultant for BeOnChip S.L. and EBERS Medical Technology S.L. (Zaragoza, Spain).

DATA AVAILABILITY STATEMENT

Research data are not shared.

ORCID

Alexander H. McMillan ⓘ https://orcid.org/0000-0001-8568-9035

Sasha Cai Lesher-Pérez ⓘ https://orcid.org/0000-0002-1740-2597

REFERENCES

1. D. T. Chiu, A. J. deMello, D. Di Carlo, P. S. Doyle, C. Hansen, R. M. Maceiczyk, R. C. R. Wootton, *Chem* **2017**, *2*, 201.

2. A. Manz, N. Graber, H. M. Widmer, *Sensors Actuators B Chem.* **1990**, *1*, 244.

3. R. Srinivasan, S. L. Firebaugh, I.-M. Hsing, J. Ryley, M. P. Harold, K. F. Jensen, M. A. Schmidt, in *Proc. Int. Solid State Sensors Actuators Conf. (Transducers '97)*, IEEE, n.d., pp. 163–166.

4. W. Ehrfeld, K. Golbig, V. Hessel, H. Löwe, T. Richter, *Ind. Eng. Chem. Res.* **1999**, *38*, 1075.

5. M. C. Mitchell, V. Spikmans, A. Manz, A. J. de Mello, *J. Chem. Soc. Perkin Trans.* **2001**, *1* 514.

6. E. Garcia-Egido, S. Y. F. Wong, B. H. Warrington, *Lab Chip* **2002**, *2*, 31.

7. T. Illg, V. Hessel, P. Lçb, J. C. Schouten, *ChemSusChem* **2011**, *4*, 392.

8. T. Asai, A. Takata, Y. Ushiogi, Y. Iinuma, A. Nagaki, J. Yoshida, *Chem. Lett.* **2011**, *40*, 393.

9. J. Pelleter, F. Renaud, *Org. Process Res. Dev.* **2009**, *13*, 698.

10. L. Vaccaro, D. Lanari, A. Marrocchi, G. Strappaveccia, *Green Chem.*. **2014**, *16*, 3680.

11. K. S. Elvira, X. C. i Solvas, R. C. R. Wootton, A. J. DeMello, *Nat. Chem.* **2013**, *5*, 905.

12. N. Convery, N. Gadegaard, *Micro NanoEng.* **2019**, *2*, 76.

13. H. Becker, C. Gärtner, *Electrophoresis* **2000**, *21*, 12.

14. S. C. Jacobson, R. Hergenroder, L. B. Koutny, J. M. Ramsey, *Anal. Chem.* **1994**, *66*, 1114.

15. D. J. Harrison, K. Fluri, K. Seiler, Z. Fan, C. S. Effenhauser, A. Manz, *Science (80-.)*. **1993**, *261*, 895.

16. C. Hnatovsky, R. S. Taylor, E. Simova, P. P. Rajeev, D. M. Rayner, V. R. Bhardwaj, P. B. Corkum, *Appl. Phys. A Mater. Sci. Process.* **2006**, *84*, 47.

17. N. Burshtein, S. T. Chan, K. Toda-Peters, A. Q. Shen, S. J. Haward, *Curr. Opin. Colloid Interface Sci.* **2019**, *43*, 1.

18. T.-L. Chang, Z.-C. Chen, Y.-W. Lee, Y.-H. Li, C.-P. Wang, *Microelectron. Eng.* **2016**, *158*, 95.

19. S.-J. Paik, S. Byun, J.-M. Lim, Y. Park, A. Lee, S. Chung, J. Chang, K. Chun, D. "Dan" Cho, *Sensors Actuators A Phys.* **2004**, *114*, 276.

20. H. Wang, R. Foote, S. Jacobson, J. Schneibel, J. Ramsey, *Sensors Actuators B Chem.* **1997**, *45*, 199.

21. J. Liu, J. Shang, J. Tang, Q.-A. Huang, *J. Microelectromechanical Syst.* **2011**, *20*, 909.

22. D. J. Harrison, A. Manz, Z. Fan, H. Luedi, H. M. Widmer, *Anal. Chem.* **1992**, *64*, 1926.

23. A. Sayah, D. Solignac, T. Cueni, M. A. Gijs, *Sensors Actuators A Phys.* **2000**, *84*, 103.

24. Z. J. Jia, Q. Fang, Z. L. Fang, *Anal. Chem.* **2004**, *76*, 5597.

25. P. B. Allen, D. T. Chiu, *Anal. Chem.* **2008**, *80*, 7153.

26. J. N. Lee, C. Park, G. M. Whitesides, *Anal. Chem.* **2003**, *75*, 6544.

27. J. E. Mark, Ed., *Physical Properties of Polymers Handbook*, Springer New York, New York, NY **2007**.

28. R. Dangla, F. Gallaire, C. N. Baroud, *Lab Chip* **2010**, *10*, 2972.

29. V. Arcella, A. Ghielmi, G. Tommasi, *Ann. N. Y. Acad. Sci.* **2003**, *984*, 226.

30. W. R. Dolbier, *J. Fluor. Chem.* **2005**, *126*, 157.

31. F. Kotz, P. Risch, D. Helmer, B. Rapp, *Micromachines* **2018**, *9*, 115.

32. T. Hizawa, A. Takano, P. Parthiban, P. S. Doyle, E. Iwase, M. Hashimoto, *Biomicrofluidics* **2018**, *12*, 064105.

33. S. Begolo, G. Colas, J. L. Viovy, L. Malaquin, *Lab Chip* **2011**, *11*, 508.

34. K. Ren, W. Dai, J. Zhou, J. Su, H. Wu, *Proc. Natl. Acad. Sci. U. S. A.* **2011**, *108*, 8162.

35. O. Cybulski, S. Jakiela, P. Garstecki, *Lab Chip* **2016**, *16*, 2198.

36. J. P. Rolland, R. M. Van Dam, D. A. Schorzman, S. R. Quake, J. M. DeSimone, *J. Am. Chem. Soc.* **2004**, *126*, 2322.

37. C. T. Riche, C. Zhang, M. Gupta, N. Malmstadt, *Lab Chip* **2014**, *14*, 1834.

38. T. Yang, J. Choo, S. Stavrakis, A. de Mello, *Chem. – A Eur. J.* **2018**, *24*, 12078.

39. E. Sano, C. Mori, N. Matsuoka, Y. Ozaki, K. Yagi, A. Wada, K. Tashima, S. Yamasaki, K. Tanabe, K. Yano, Y. Torisawa, *Micromachines* **2019**, *10*, 793.

40. J. Lachaux, C. Alcaine, B. Gómez-Escoda, C. M. Perrault, D. O. Duplan, P.-Y. J. Wu, I. Ochoa, L. Fernandez, O. Mercier, D. Coudreuse, E. Roy, *Lab Chip* **2017**, *17*, 2581.

41. J. Lachaux, H. Salmon, F. Loisel, N. Arouche, I. Ochoa, L. L. Fernandez, G. Uzan, O. Mercier, T. Veres, E. Roy, *Adv. Mater. Technol.* **2019**, *4*, 1.

42. D. J. Case, Y. Liu, I. Z. Kiss, J. R. Angilella, A. E. Motter, *Nature* **2019**, *574*, 647.

43. E. Roy, M. Geissler, J. C. Galas, T. Veres, *Microfluid. Nanofluidics* **2011**, *11*, 235.

44. E. Roy, J. C. Galas, T. Veres, *Lab Chip* **2011**, *11*, 3193.

45. Y. Temiz, R. D. Lovchik, G. V. Kaigala, E. Delamarche, *Microelectron. Eng.* **2015**, *132*, 156.

46. E. Roy, A. Pallandre, B. Zribi, M.-C. Horny, F. D. Delapierre, A. Cattoni, J. Gamby, A.-M. Haghiri-Gosnet, in *Adv. Microfluid. - New Appl. Biol. Energy, Mater. Sci.* (Ed.: X.-Y. Yu), InTechOpen, London, UK, **2016**.

47. E. Berthier, E. W. K. Young, D. Beebe, *Lab Chip* **2012**, *12*, 1224.

48. M. D. Borysiak, K. S. Bielawski, N. J. Sniadecki, C. F. Jenkel, B. D. Vogt, J. D. Posner, *Lab Chip* **2013**, *13*, 2773.

49. M. A. Unger, H. Chou, T. Thorsen, A. Scherer, S. Quake, *Science (80-.)*. **2000**, *288*, 113.

50. P. Vulto, N. Glade, L. Altomare, J. Bablet, L. Del Tin, G. Medoro, I. Chartier, N. Manaresi, M. Tartagni, R. Guerrieri, *Lab Chip* **2005**, *5*, 158.

51. J. C. McDonald, D. C. Duffy, J. R. Anderson, D. T. Chiu, H. Wu, O. J. A. Schueller, G. M. Whitesides, *Electrophoresis* **2000**, *21*, 27.

52. M. A. Eddings, M. A. Johnson, B. K. Gale, *J. Micromechanics Microengineering* **2008**, *18*, 067001.

53. S. Bhattacharya, A. Datta, J. M. Berg, S. Gangopadhyay, *J. Microelectromechanical Syst.* **2005**, *14*, 590.

54. R. Novak, C. F. Ng, D. E. Ingber, in *Cell-Based Microarrays. Methods Mol. Biol.* Vol *1771* (Eds.: P. Ertl, M. Rothbauer), Humana Press, New York, NY **2018**, pp. 161–170.

55. C. Hansen, *Hansen Solubility Parameters*, CRC Press, **2007**.

56. W. A. Woishnis, S. Ebnesajjad, *Chemical Resistance of Thermoplastics*, Elsevier, Oxford **2012**.

57. J. H. Hildebrand, R. S. Scott, *The Solubility of Nonelectrolytes* (Eds: J. H. Hildebrand, R. S. Scott), Reinhold Pub. Corp., New York **1950**.

58. J. Lara, D. Drolet, C. Hansen, A. Chollot, N. Monta, *Int. J. Curr. Res.* **2017**, *9*, 47860.

59. M. Vayer, A. Vital, C. Sinturel, *Eur. Polym. J.* **2017**, *93*, 132.

60. G. A. Diaz-Quijada, R. Peytavi, A. Nantel, E. Roy, M. G. Bergeron, M. M. Dumoulin, T. Veres, *Lab Chip* **2007**, *7*, 856.

61. D. Ogończyk, J. Węgrzyn, P. Jankowski, B. Dąbrowski, P. Garstecki, *Lab Chip* **2010**, *10*, 1324.

62. A. Piruska, I. Nikcevic, S. H. Lee, C. Ahn, W. R. Heineman, P. A. Limbach, C. J. Seliskar, *Lab Chip* **2005**, *5*, 1348.

63. Y. Hanada, T. Ogawa, K. Koike, K. Sugioka, *Lab Chip* **2016**, *16*, 2481.

64. A. K. Au, W. Lee, A. Folch, *Lab Chip* **2014**, *14*, 1294.

65. D. N. H. Kim, K. T. Kim, C. Kim, M. A. Teitell, T. A. Zangle, *Microfluid. Nanofluidics* **2018**, *22*, 1.

66. S. H. Hamid, W. H. Prichard, *Polym. Plast. Technol. Eng.* **1988**, *27*, 303.

67. E. Yousif, R. Haddad, *Springerplus* **2013**, *2*, 398.

68. A. Mata, A. J. Fleischman, S. Roy, *Biomed. Microdevices* **2005**, *7*, 281.

69. S. Deguchi, J. Hotta, S. Yokoyama, T. S. Matsui, *J. Micromechanics Microengineering* **2015**, *25*, 097002.

70. I. D. Johnston, D. K. McCluskey, C. K. L. Tan, M. C. Tracey, *J. Micromechanics Microengineering* **2014**, *24*, 035017.

71. H. A. Stone, A. D. Stroock, A. Ajdari, *Annu. Rev. Fluid Mech.* **2004**, *36*, 381.

72. Q. Kang, D. Zhang, S. Chen, *J. Fluid Mech.* **2005**, *545*, 41.

73. A. Nabizadeh, M. Adibifard, H. Hassanzadeh, J. Fahimpour, M. Keshavarz Moraveji, *J. Mol. Liq.* **2019**, *273*, 248.

74. B. Zhao, C. W. MacMinn, R. Juanes, *Proc. Natl. Acad. Sci. U. S. A.* **2016**, *113*, 10251.

75. M. P. Boruah, A. Sarker, P. R. Randive, S. Pati, S. Chakraborty, *Phys. Fluids* **2018**, *30*, 122106.

76. F. M. Fowkes, *Ind. Eng. Chem.* **1964**, *56*, 40.

77. M. J. Owen, *Comments Inorg. Chem.* **1988**, *7*, 195.

78. J. B. Taylor, A. L. Carrano, S. G. Kandlikar, *Int. J. Therm. Sci.* **2006**, *45*, 962.

79. B. Dai, M. Li, Y. Ma, *Appl. Therm. Eng.* **2014**, *67*, 283.

80. J. Jia, Q. Song, Z. Liu, B. Wang, *Microsyst. Technol.* **2019**, *25*, 2385.

81. T. Wang, J. Wu, T. Chen, F. Li, T. Zuo, S. Liu, *Microsyst. Technol.* **2017**, *23*, 1405.

82. E. Vereshchagina, P. Carmona, E. Andreassen, J. Batalden, M. Plassen, M. M. Mielnik, *Proc. IEEE Int. Conf. Micro Electro Mech. Syst.* **2018**, *2018*, 1257.

83. C. Matellan, A. E. Del Río Hernández, *Sci. Rep.* **2018**, *8*, 6971.

84. I. R. G. Ogilvie, V. J. Sieben, C. F. A. Floquet, R. Zmijan, M. C. Mowlem, H. Morgan, *J. Micromechanics Microengineering* **2010**, *20*, 065016.

85. M. W. Toepke, D. J. Beebe, *Lab Chip* **2006**, *6*, 1484.

86. M. D. Brennan, M. L. Rexius-Hall, L. J. Elgass, D. T. Eddington, *Lab Chip* **2014**, *14*, 4305.

87. M. B. Plutschack, B. Pieber, K. Gilmore, P. H. Seeberger, *Chem. Rev.* **2017**, *117*, 11796.

88. T. C. Merkel, V. I. Bondar, K. Nagai, B. D. Freeman, I. Pinnau, *J. Polym. Sci. Part B Polym. Phys.* **2000**, *38*, 415.

89. H. X. Rao, F. N. Liu, Z. Y. Zhang, *J. Memb. Sci.* **2007**, *303*, 132.

90. Y. Q. Fan, H. L. Wang, K. X. Gao, J. J. Liu, D. P. Chai, Y. J. Zhang, *Chinese J. Anal. Chem.* **2018**, *46*, 1863.

91. C.-W. Tsao, *Micromachines* **2016**, *7*, 225.

92. A. H. McMillan, E. K. Thomée, A. Dellaquila, H. Nassman, T. Segura, S. C. Lesher-Pérez, *Micromachines* **2020**, *11*, 731.

93. J. Schindelin, I. Arganda-Carreras, E. Frise, V. Kaynig, M. Longair, T. Pietzsch, S. Preibisch, C. Rueden, S. Saalfeld, B. Schmid, J. Y. Tinevez, D. J. White, V. Hartenstein, K. Eliceiri, P. Tomancak, A. Cardona, *Nat. Methods* **2012**, *9*, 676.

94. E. C. Harrington, *Ind. Qual. Control* **1965**, *21*, 494.

95. I. Horcas, R. Fernández, J. M. Gómez-Rodríguez, J. Colchero, J. Gómez-Herrero, A. M. Baro, *Rev. Sci. Instrum.* **2007**, *78*, 013705.

96. A. L. Khan, S. Basu, A. Cano-Odena, I. F. J. Vankelecom, *J. Memb. Sci.* **2010**, *354*, 32.

97. J. Didden, R. Thür, A. Volodin, I. F. J. Vankelecom, *J. Appl. Polym. Sci.* **2018**, *135*, 1.

98. R. Thür, N. Van Velthoven, S. Slootmaekers, J. Didden, R. Verbeke, S. Smolders, M. Dickmann, W. Egger, D. De Vos, I. F. J. Vankelecom, *J. Memb. Sci.* **2019**, *576*, 78.

SUPPORTING INFORMATION

Additional supporting information may be found online in the Supporting Information section at the end of the article.

How to cite this article: McMillan AH, Mora-Macías J, Teyssandier J, et al. Self-sealing thermoplastic fluoroelastomer enables rapid fabrication of modular microreactors. *Nano Select*. **2021**;*2*:1385–1402. https://doi.org/10.1002/nano.202000241